Background nutrient concentration determines phytoplankton bloom response to marine heatwaves

Hakase Hayashida[1,2*], Richard J. Matear[2,3], and Peter G. Strutton[1,2]

[1]Institute for Marine and Antarctic Studies, University of Tasmania, Hobart, Tasmania, Australia
[2]Australian Research Council Centre of Excellence for Climate Extremes, University of Tasmania, Hobart, Tasmania, Australia
[3]CSIRO Oceans and Atmosphere, Hobart, Tasmania, Australia
*Corresponding author: hakase.hayashida@utas.edu.au

Abstract

Ocean temperature extreme events such as marine heatwaves are expected to intensify in coming decades due to anthropogenic global warming. Reported ecological and economic impacts of marine heatwaves include coral bleaching, local extinction of mangrove and kelp forests, and elevated mortalities of invertebrates, fishes, seabirds, and marine mammals. In contrast, little is known about the impacts of marine heatwaves on microbes that regulate biogeochemical processes in the ocean. Here we analyze the daily output of a near-global ocean physical-biogeochemical model simulation to characterize the impacts of marine heatwaves on phytoplankton blooms in 23 tropical and temperate oceanographic regions from 1992 to 2014. The results reveal regionally-coherent anomalies of shallower mixed layers and lower surface nitrate concentrations during marine heatwaves. Strengthened stratification is the plausible cause of such responses that exert counteracting effects on phytoplankton growth through light and nutrient limitation. Consequently, the responses of phytoplankton blooms are mixed, but can be related to the background nutrient conditions of the study regions. With one exception, blooms are weaker during marine heatwaves in nutrient poor waters, whereas in nutrient rich waters, the heatwave blooms are stronger. The corresponding analyses of sea-surface temperature and chlorophyll *a* concentration based on satellite observations support this relationship between phytoplankton bloom anomalies and background nitrate concentration. Given that nutrient poor waters are projected to expand globally in the twenty-first century, this study suggests increased occurrence of weaker blooms during marine heatwaves in coming decades, with implications for higher trophic levels and biogeochemical cycling of key elements.

1 Introduction

Marine heatwaves refer to prolonged anomalous warming events in the ocean that last for days, months, and in some extreme cases, years (Hobday et al., 2018). These events have negative impacts on marine organisms that are vulnerable to transient ocean warming. Reported ecological and economic impacts of marine heatwaves include coral bleaching, local extinction of mangrove and kelp forests, and elevated mortalities of invertebrates, fishes, seabirds, and marine mammals (Smale et al., 2019).

Although the influence of marine heatwaves on large plants and animals is well documented, the literature on the impacts on lower trophic levels is both scant and inconclusive. For example, monthly shipboard measurements of phytoplankton and zooplankton (copepods) abundance and composition on the Alaskan Shelf have revealed a significant positive correlation between temperature and the abundance of diatoms and copepods during 2000-2015, except for the last two years corresponding to the northeast Pacific 'blob' event (Batten et al., 2018). Monthly satellite chlorophyll *a* observations have demonstrated both positive and negative phytoplankton biomass anomalies in the northeast Pacific, depending on both time and location (Cavole et al., 2016).

The major challenge of marine heatwave studies on lower trophic levels is the lack of high-resolution and long-term monitoring of environmental and biological variables, such as mixed layer depth, nutrient concentration, and biomass of phytoplankton and zooplankton. Daily resolution is needed because some extreme events only last for days. On the other hand, decades of measurements are needed to establish a well-defined baseline for distinguishing marine heatwave impacts from interannual variability (Hobday et al., 2016). Having such measurements is essential to develop a mechanistic understanding of the effects of marine heatwaves on ocean biogeochemistry. For these reasons, biogeochemical models and satellite observations are perhaps best suited to this type of study.

In this study, we characterize the impacts of marine heatwaves on phytoplankton blooms using model simulation and satellite observations over recent decades. Model simulation allows us to analyze the variability in physical and biogeochemical variables that are practically impossible to obtain observationally at the daily temporal resolution and decadal time period needed for quantifying marine heatwave impacts. On the other hand, satellite observations provide a means of verification of simulated marine heatwaves and their impacts on phytoplankton blooms.

2 Materials and methods

2.1 Study regions

We define 23 oceanographic regions for diagnosing simulated and observed marine heatwave events and their effects on physical and biogeochemical properties (Figure 1). These regions are selected in order to provide a global perspective, encompassing both tropical and temperate waters, western and eastern boundary currents, nutrient limited and replete waters, and coastal and open-water areas. Furthermore, many of these regions have experienced marine heatwaves in recent decades, and some of their drivers and socio-economic impacts have been assessed in the literature (Hobday et al., 2018; Holbrook et al., 2019).

2.2 Marine heatwave definition

We define an ocean warming event as a marine heatwave when the daily-mean sea surface temperature exceeds its climatological 90th percentile for at least 5 days. This definition follows that of Hobday et al. (2016) which was developed to facilitate comparisons among the literature. We define 1982-2014 as the climatological period based on the availability of both the model and satellite data products of daily-mean sea surface temperature. Following Hobday et al. (2016), the daily climatological 90th percentile is defined after smoothing the time series with 30-day moving averages. To characterize marine heatwave events, we use the following metrics: frequency, duration, mean intensity, annual MHW days, and category (Hobday et al., 2018).

2.3 Model data products

We analyze the output of three numerical experiments (historical, projection, and control) conducted using the Ocean Forecasting Australian Model version 3 (OFAM3), which is documented in detail in Zhang et al. (2016, 2017). In brief, OFAM3 is a near-global configuration of the Modular Ocean Model version 4.1 (Griffies, 2010), which extends from 75° S to 75° N with a spatial resolution of 0.1°. At this resolution, the model resolves mesoscale eddies in most of the tropical and temperate regions (Hallberg, 2013). OFAM3 does not have a prognostic sea-ice model component, but incorporates satellite-derived sea-ice concentration as surface boundary conditions. There are 51 non-uniform vertical layers, with the finest resolution of 5 m in the uppermost layer. OFAM3 has a biogeochemistry model component called the Whole Ocean Model with Biogeochemistry and Trophic-dynamics (WOMBAT; Oke et al., 2013). WOMBAT simulates five state variables representative of the lower-trophic-level ecosystem: nitrate, iron, phytoplankton, zooplankton, and detritus. The model equations are described in detail in Oke et al. (2013) and the parameters are set to those adapted for the Australian Community Climate and Earth System Simulator (ACCESS-ESM1; Law et al., 2017). The growth rate of phytoplankton depends on temperature, light, nitrate, and iron. Specifically, the temperature determines the maximum specific growth rate similar to the Eppley curve (Eppley, 1972), whereas reduced light or nutrient conditions can limit the growth rate similar to the Monod equation (Monod, 1949). Although iron can be a limiting factor for phytoplankton growth in the model, our preliminary analysis indicates that it is never limiting in the model simulation (Figure S1), and therefore we exclude iron from the rest of the analysis.

To diagnose simulated marine heatwave events in the 23 study regions, we obtain the daily- and regional-mean time series of simulated sea-surface temperature from 1982 to 2014 of the historical experiment. This experiment is driven by the interannual near-surface atmospheric forcing fields based on the Japanese 55-year Atmospheric Reanalysis (JRA-55; Kobayashi et al., 2015) after 20 years of model spin-up (Zhang et al., 2016).

To diagnose the variability in physical and biogeochemical properties during marine heatwave events, we obtain the daily- and regional-mean time series of simulated mixed layer depth (MLD), sea-surface nitrate concentration, sea-surface phytoplankton and zooplankton biomass, and depth-integrated gross primary production from 1992 to 2014 of the historical experiment, during which ocean biogeochemistry is simulated. Due to the short duration of the model experiment, the model drift is unavoidable for biogeochemical variables even in the ocean surface layer. To resolve this issue, we estimate the model drift from the control experiment, which is done in parallel with the historical experiment, and remove the drift from the time series of the historical experiment (see Supplementary Information). Note that simulated physical properties, including sea-surface temperature and mixed layer depth, do not experience such a drift due to the set-up of the model spin-up as demonstrated by Zhang et al. (2016).

To address marine heatwave impacts under the future climate, we obtain the annual-mean fields of simulated sea-surface nitrate concentration of the projection experiment. This experiment spans 2006 to 2101, driven by an atmospheric forcing that has both the interannual variability of JRA55 and the long-term global warming trend derived by an ensemble mean of the Coupled Model Intercomparison Project phase 5 (CMIP5) Representative Concentration Pathway 8.5 (RCP8.5) projections (Zhang et al., 2017).

2.4 Satellite data products

To evaluate the model simulation of marine heatwaves, we obtain the daily-mean sea-surface temperature reanalysis product of the Merged satellite and in situ data Global Daily Sea Surface Temperature (MGD SST; Kurihara et al., 2006). This data product is representative of ocean temperature at foundation depth (5-10 m; Fiedler et al., 2019; Kawai and Wada, 2007), which is closer to the representative depth of OFAM3 (2.5 m) than that of the National Oceanic and Atmospheric Administration Optimum Interpolation Sea Surface Temperature version 2 (NOAA OISST2), which is about 0.5 m (Reynolds et al., 2007). OFAM3 simulates marine heatwaves that are in reasonable spatial agreement with both MGD SST and NOAA OISST2, but it compares better with MGD SST than NOAA OISST2 in terms of annual marine heatwave days (Hayashida et al., submitted).

To examine the variability in observed phytoplankton biomass during marine heatwave events and compare it with model simulation, we obtain the daily-mean sea-surface chlorophyll *a* concentration from 2002 to 2018 derived from the Moderate Resolution Imaging Spectroradiometer Aqua (MODIS hereafter) ocean colour sensor. This data product is obtained through the GlobColour project (http://www.globcolour.info/; accessed on August 19, 2019) at the spatial resolution of 1°, which is sufficient for the 23 study regions defined in the present study.

Although a merged product of multiple ocean colour sensors is available for longer temporal coverage, our preliminary analysis demonstrates substantial differences in chlorophyll *a* concentration estimates between MODIS and the Sea-Viewing Wide Field-of-View Sensor

(SeaWiFS hereafter, operational 1997 to 2010) for most of the study regions (Figures S3-25). The differences are systematic in that MODIS provides higher values during bloom seasons, which is consistent with the finding of Marrari et al. (2016) for the South Atlantic Ocean. For this reason, we use the data product based on a single sensor (MODIS, because it has a longer record than SeaWiFS) rather than a merged product.

2.5 In situ climatology

To compare the simulated nutrients with observations, we obtain the 1° global annual-mean climatological sea-surface nitrate concentration field of the World Ocean Atlas 2013 version 2 (WOA13; Garcia et al., 2013). In particular, we analyze the statistical mean product, which is the average of all unflagged interpolated values in each grid cell which contain at least one measurement.

3 Results

Here we focus on the mean characteristics of marine heatwave metrics and the mean anomalies of mixed layer depth, sea-surface nitrate concentration, sea-surface phytoplankton biomass, and sea-surface chlorophyll *a* concentration in the 23 study regions for periods when phytoplankton blooms and marine heatwaves co-occur. The term mean refers to climatological representation over the period 1992-2014 for all variables with the exception of sea-surface chlorophyll *a* concentration anomalies, which are representative of the MODIS period (2002-2018). The anomalies are expressed as standardized anomalies (SA), which are the differences from the daily-mean climatologies divided by the interannual standard deviations. Phytoplankton blooms are defined for each region as the period from the day of the annual minimum to its annual maximum in the daily-mean climatology of sea-surface phytoplankton biomass or chlorophyll *a* concentration (Figure S2). Comparisons of daily- and regional-mean time series of the aforementioned variables and individual marine heatwave events between the model and observations are provided in Figures S3-29.

3.1 Simulated and observed marine heatwaves

From 1992 to 2014 in the model, the study regions experience on average at least one marine heatwave event per year that is about 30 days long and 0.75 °C above the daily-mean climatology (Figure 2). These numbers compare well with observations that show about two events per year with each event lasting for nearly 20 days and about 1 °C warmer than the normal condition. The model and observations agree exceptionally well in terms of the number of marine heatwave days per year averaged over the study regions (33.7 days; Figure 2d). Both the model and observations agree that marine heatwaves occur throughout the year for all regions with generally higher probabilities in summer seasons. Typically, more events result in a shorter duration for each event and vice versa, as indicated by statistically-significant and highly-negative correlations between the mean frequency and duration over the 23 study regions (r^2 = -0.64 and -0.87 for the model and observations, respectively, with p-value < 0.05 for both).

Comparisons for each study region reveal a few notable similarities and differences between the model and observations. The model and observations agree in terms of the occurrence of a marine heatwave event in the Galapagos Island region which is categorized as "extreme" (Figures 2a and S13). This event is known to have occurred as a result of a strong El Niño in 1997-1998 (Holbrook et al., 2019). The model simulates two additional extreme heatwave events for the Leeuwin Current and South China Sea, whereas the observations do not categorize these as extreme (Figures S9 and S5, respectively). This Leeuwin Current warming in 2011 is known to have been caused by a strong La Niña (Feng et al., 2013) and while the observations used here did not classify it as extreme, it is well-documented to have had far-reaching and serious impacts on the marine environment (Wernberg et al., 2013).

The model simulates on average less than one marine heatwave event per year for the Atlantic Equatorial Current and Humboldt Current regions, whereas the observations show more than two events per year for these regions (Figure 2a). These differences in the mean frequency are related to differences in the mean duration, which are about 45 days longer in the model for both regions. Furthermore, the model simulates substantially longer marine heatwaves for the California Current and Scotian Shelf and Grand Banks regions. The model shows a wider spread in the mean duration distribution across the study regions, as indicated by higher standard deviation (17.6 vs. 4.5 days for the model and observations, respectively).

The mean intensity of simulated marine heatwaves is lower than that of observed marine heatwaves for all regions (Figure 2c). The largest difference of approximately 0.5 °C occurs for the Scotian Shelf and Grand Banks region. This region also differs the greatest between the model and observations among all study regions in terms of the mean marine heatwave days (22.2 days more for the model; Figure 2d).

3.2 Simulated mixed layer depth, sea-surface nitrate concentration, and sea-surface phytoplankton biomass

In the historical experiment of OFAM3, the co-occurrence of simulated marine heatwaves and phytoplankton blooms takes place on average about once a year and lasts for 26 days during 1992-2014 (Figure 3a). The anomalies of simulated mixed layer depth during the marine heatwave-phytoplankton bloom co-occurrence are negative, meaning shallower than average, for all study regions except for the Bay of Bengal and California Current regions (Figure 3b). Seven of these regions experience exceptionally shallow mixed layers as indicated by the magnitudes exceeding one. Similarly, the anomalies of simulated sea-surface nitrate concentration are negative, meaning lower than average, for all regions (Figure 3c). Eleven of these regions experience exceptionally low nitrate levels. Among these regions, four experience both anomalously shallow mixed layers and low nutrient levels. Shallower mixed layers imply relaxation from light limitation, whereas lower nitrate concentration exacerbates nutrient limitation. Hence, these two anomalies have counteracting effects on photosynthetic growth: enhancing light exposure but reducing nutrient supply. Consequently, the anomalies of simulated phytoplankton biomass are both positive and negative across the study regions (Figure 3d), depending on which resource — light or nutrients — is more strongly limiting or whose limitation is more completely relieved. Five of these regions experience exceptionally high or low biomass. Note that these anomalies are strongly correlated with the anomalies of both sea-surface zooplankton biomass and depth-integrated gross primary production across the study regions (Figure S30).

3.3 Observed sea-surface chlorophyll *a* concentration

Similar to the model simulation, the co-occurrence of observed marine heatwaves and phytoplankton blooms defined based on the combination of MGD and MODIS takes place roughly once a year, but lasts for 18 days on average during 2002-2018 (Figure 4a). The duration is about a week shorter than the model simulation, which is partly due to the shorter duration of marine heatwaves in general (Figure 2b) and may also be due to the shorter duration of phytoplankton blooms in some regions (Figure S2). As in the simulated phytoplankton biomass, the anomalies of observed sea-surface chlorophyll *a* concentration are both positive and negative (Figure 4b). On the other hand, the magnitudes of the observed anomalies are smaller than the simulated anomalies. The observed magnitudes are relatively high (exceeding 0.5) in 6 regions.

3.4 Relationship between phytoplankton bloom response and background nutrient concentration

To further investigate the mixed responses of simulated and observed phytoplankton blooms to marine heatwaves, the anomalies are plotted against the climatological annual-mean sea-surface nitrate concentration across the study regions (Figure 5). Doing so reveals a remarkable relationship that is common to both the model simulation and observations. All of the negative anomalies take place in regions where nitrate concentration is less than 3 μM, while the anomalies are positive for all regions where nitrate concentration is greater than 3 μM. The only exceptions are the simulated and observed negative anomalies for the Galapagos Island region, where nitrate concentration is greater than 3 μM.

More broadly speaking, these findings distinguish the impacts of marine heatwaves on phytoplankton blooms between nutrient limited and replete waters. As demonstrated by the model results in Section 3.2, marine heatwaves are typically associated with shallower mixed layer depth and lower nitrate concentration. In nutrient limited waters, these conditions exacerbate nutrient stress, resulting in weaker blooms. In contrast, in nutrient replete waters, the reduced nitrate concentration associated with marine heatwaves is not low enough to limit photosynthetic growth. Instead, light is presumably the limiting factor in these regions, and therefore marine heatwaves are generally associated with stronger blooms owing to shallower mixed layer depth and the relief of light limitation.

Despite high background nutrient concentration, both the model simulation and observations demonstrate that marine heatwaves in the Galapagos Island region are associated with weaker blooms. These unexpected results are driven by extremely strong El Niño events (1997-1998 during the model simulation period and 2015-2016 during the MODIS observation period; Figures S9, S27, and S31), which drive weakened or absent upwelling of nutrient rich waters (Chavez et al., 1999). That is, unlike the other high nutrient (>3 μM) regions, marine heatwaves (El Niño events) around the Galapagos can suppress nutrients to the point of nutrient limitation. The weaker bloom during the 1997-1998 El Niño in the model simulation is consistent with the SeaWiFS observations (Ryan et al., 2002).

Lastly, we note the regime in which nutrient poor regions experience stronger blooms during marine heatwaves (the top-left quadrant of Figure 5). A few possible explanations for this regime are: (1) the region is light limited rather than nutrient limited because of seasonal and interannual variability that relieves the nutrient limited conditions, so that blooms are larger due to relaxed light limitation; and (2) the effect of temperature on the photosynthetic growth rate is greater than that of nutrient limitation. Separating the two effects requires more thorough analyses of budget components.

3.5 Simulated sea-surface nitrate concentration in the twenty-first century

Under global warming, the spatial distribution of background nutrient concentration is projected to change throughout the twenty-first century. The model simulation based on the RCP8.5 scenario shows an expansion of nutrient poor waters (Figure 6). More specifically, the spatial extent of simulated nutrient poor waters (defined here as less than 3μM nitrate) in the 60 ºS-60 ºN surface ocean is projected to increase by 8 % during the late twenty-first century (2071-2100) compared to the early twenty-first century (2006-2035). Among the 23 study regions, this projected change has implications for four regions (the Bay of Bengal, Galapagos Island, Northwest Pacific, and Tasmania) where the area of nutrient poor waters increases noticeably. Based on our analysis of the co-occurrence of marine heatwaves and phytoplankton blooms, the projected change would move these systems out of the top-right quadrant of Figure 5, and into the bottom-left quadrant. Therefore, in the future these regions would show a reduction in phytoplankton blooms during marine heatwaves. The projected expansion of nutrient poor surface waters is also present in 7 out of 8 CMIP5 models with similar percentage changes (1-5 %; Figure S32).

4 Discussion

Climate extreme events like marine heatwaves are occurring at an unprecedented and extensive rate (Babcock et al., 2019), and they may have greater ecological impacts than the more gradual effects of climate change. Here we combine observations and simulations to elucidate the impacts of marine heatwaves on phytoplankton dynamics. Our model simulation shows that marine heatwave events in the 23 study regions are generally associated with shallower mixed layers and lower nitrate. These two responses have counteracting effects on phytoplankton growth; shallower mixed layer depth can increase growth by relaxing light limitation, whereas lower nitrate concentration can reduce the growth by amplifying nutrient stress. The relative importance of these factors, and therefore the phytoplankton bloom response during marine heatwaves, varies regionally, but we find that it is linked to background nutrient concentration. Weaker blooms are almost always associated with marine heatwaves in nutrient poor regions, and vice versa. This finding is robust. Our analyses based on satellite observations support the model results in spite of differences in biomass proxies (nitrogen content vs. chlorophyll *a* concentration) and temporal coverages (1994-2014 for model vs. 2002-2018 for satellite).

Although not named as marine heatwaves, a few previous studies have documented lower phytoplankton biomass and primary productivity during comparable transient ocean warming events around the Galapagos Island region (Ryan et al., 2002), in the southern California Current (Cavole et al., 2016; Zaba and Rudnick, 2016), the northeast Pacific (Kudela et al., 2006), and the northern Humboldt Current (Iriarte and González, 2004). Our simulated and observed results are consistent with these previous studies for the Galapagos Islands, California Current, and British Columbia Continental Shelf (corresponding to the northeast Pacific) regions. However, unlike Iriarte and González (2004), our simulated phytoplankton biomass in the Humboldt Current region during the 1997-1998 El Niño is not lower than the climatology, most probably due to the positive bias in background nutrient concentration in the model, and so phytoplankton growth is not limited by nutrients. Hence, in addition to phytoplankton anomalies, our model results provide evidence for nutrient limitation during marine heatwaves due to strengthened stratification in these coastal upwelling systems of the eastern Pacific.

Our simulated and observed findings are applicable to total phytoplankton only, but the responses of different functional types and size classes are presumably variable, because growth rates as a function of temperature, light, and nutrient conditions, are variable. Previous studies have reported a transient change to a small-cell dominated phytoplankton community composition during ocean warming events (Iriarte and González, 2004; Kudela et al., 2006) that has implications for higher trophic levels (Jones et al., 2018). Similarly, the limitation of other macro- and micro-nutrients is disregarded in the present study. Accounting for this process can again affect the community composition (e.g. silicate deficiency is only relevant for diatoms) and may hasten and amplify the negative bloom anomalies in iron limited regions. However, these considerations should not change the conclusion about the general relationship between phytoplankton bloom response and background nutrient concentration. More detailed analyses on these topics can be performed using a more complex ocean biogeochemistry model. Lastly, while our study mostly concerns the variability of sea-surface properties, investigating the vertical structures of marine heatwaves and associated biogeochemical properties (Zaba and Rudnick, 2016) would be worthwhile, to comprehend the impacts throughout the water column. Such a study could be achieved through process studies or deployments of autonomous platforms such as floats and gliders.

The impacts of marine heatwaves on phytoplankton are more than just the thermal stress, and therefore are more complex than the impacts on large plants and higher trophic levels. Strengthened stratification is a key mechanism for phytoplankton anomalies during marine heatwaves. Although stronger blooms could be associated with marine heatwaves, projected expansion of nutrient poor waters suggests increased occurrence of weaker blooms in coming decades, with implications for higher trophic levels and biogeochemical cycling of key elements. Through a synthesis of simulated and observed regional-mean time series analyses, this study offers insights into a relationship between marine heatwaves and ocean biogeochemistry.

References

Babcock, R.C., Bustamante, R.H., Fulton, E.A., Fulton, D.J., Haywood, M.D.E., Hobday, A.J., Kenyon, R., Matear, R.J., Plagányi, E.E., Richardson, A.J., et al. (2019). Severe Continental-Scale Impacts of Climate Change Are Happening Now: Extreme Climate Events Impact Marine Habitat Forming Communities Along 45% of Australia's Coast. Front. Mar. Sci. *6*.

Batten, S.D., Raitsos, D.E., Danielson, S., Hopcroft, R., Coyle, K., and McQuatters-Gollop, A. (2018). Interannual variability in lower trophic levels on the Alaskan Shelf. Deep Sea Res. Part II Top. Stud. Oceanogr. *147*, 58–68.

Cavole, L.M., Demko, A., Giddings, A., Koester, I., Pagniello, C., Paulsen, M.-L., Ramirez-Valdez, A., Schwenck, S., Yen, N., Zill, M., et al. (2016). Biological Impacts of the 2013–2015 Warm-Water Anomaly in the Northeast Pacific: Winners, Losers, and the Future. Oceanography *29*.

Chavez, F.P., Strutton, P.G., Friederich, G.E., Feely, R.A., Feldman, G.C., Foley, D.G., and McPhaden, M.J. (1999). Biological and Chemical Response of the Equatorial Pacific Ocean to the 1997-98 El Niño. Science *286*, 2126–2131.

Eppley, R.W. (1972). Temperature and phytoplankton growth in the sea. Fish Bull *70*, 1063–1085.

Feng, M., McPhaden, M.J., Xie, S.-P., and Hafner, J. (2013). La Niña forces unprecedented Leeuwin Current warming in 2011. Sci. Rep. *3*, 1277.

Fiedler, E.K., McLaren, A., Banzon, V., Brasnett, B., Ishizaki, S., Kennedy, J., Rayner, N., Roberts-Jones, J., Corlett, G., Merchant, C.J., et al. (2019). Intercomparison of long-term sea surface temperature analyses using the GHRSST Multi-Product Ensemble (GMPE) system. Remote Sens. Environ. *222*, 18–33.

Garcia, H.E., Locarnini, R.A., Boyer, T.P., Antonov, J.I., Baranova, O.K., Zweng, M.M., Reagan, J.R., Johnson, D.R., Mishonov, A.V., and Levitus, S. (2013). World ocean atlas 2013. Volume 4, Dissolved inorganic nutrients (phosphate, nitrate, silicate).

Griffies, S.M. (2010). ELEMENTS OF MOM4P1 (NOAA/Geophysical Fluid Dynamics Laboratory).

Hallberg, R. (2013). Using a resolution function to regulate parameterizations of oceanic mesoscale eddy effects. Ocean Model. *72*, 92–103.

Hobday, A., Oliver, E., Sen Gupta, A., Benthuysen, J., Burrows, M., Donat, M., Holbrook, N., Moore, P., Thomsen, M., Wernberg, T., et al. (2018). Categorizing and Naming Marine Heatwaves. Oceanography *31*.

Hobday, A.J., Alexander, L.V., Perkins, S.E., Smale, D.A., Straub, S.C., Oliver, E.C.J., Benthuysen, J.A., Burrows, M.T., Donat, M.G., Feng, M., et al. (2016). A hierarchical approach to defining marine heatwaves. Prog. Oceanogr. *141*, 227–238.

Holbrook, N.J., Scannell, H.A., Gupta, A.S., Benthuysen, J.A., Feng, M., Oliver, E.C.J., Alexander, L.V., Burrows, M.T., Donat, M.G., Hobday, A.J., et al. (2019). A global assessment of marine heatwaves and their drivers. Nat. Commun. *10*, 2624.

Iriarte, J.L., and González, H.E. (2004). Phytoplankton size structure during and after the 1997/98 El Niño in a coastal upwelling area of the northern Humboldt Current System. Mar. Ecol. Prog. Ser. *269*, 83–90.

Jones, T., Parrish, J.K., Peterson, W.T., Bjorkstedt, E.P., Bond, N.A., Ballance, L.T., Bowes, V., Hipfner, J.M., Burgess, H.K., Dolliver, J.E., et al. (2018). Massive Mortality of a Planktivorous Seabird in Response to a Marine Heatwave. Geophys. Res. Lett. *45*, 3193–3202.

Kawai, Y., and Wada, A. (2007). Diurnal sea surface temperature variation and its impact on the atmosphere and ocean: A review. J. Oceanogr. *63*, 721–744.

Kobayashi, S., Ota, Y., Harada, Y., Ebita, A., Moriya, M., Onoda, H., Onogi, K., Kamahori, H., Kobayashi, C., Endo, H., et al. (2015). The JRA-55 Reanalysis: General Specifications and Basic Characteristics. J. Meteorol. Soc. Jpn. Ser II *93*, 5–48.

Kudela, R.M., Cochlan, W.P., Peterson, T.D., and Trick, C.G. (2006). Impacts on phytoplankton biomass and productivity in the Pacific Northwest during the warm ocean conditions of 2005. Geophys. Res. Lett. *33*.

Kurihara, Y., Sakurai, T., and Kuragano, T. (2006). Global daily sea surface temperature analysis using data from satellite microwave radiometer, satellite infrared radiometer and in-situ observations. Weather Bull. *73*, 1–18.

Law, R.M., Ziehn, T., Matear, R.J., Lenton, A., Chamberlain, M.A., Stevens, L.E., Wang, Y.-P., Srbinovsky, J., Bi, D., Yan, H., et al. (2017). The carbon cycle in the Australian Community Climate and Earth System Simulator (ACCESS-ESM1) – Part 1: Model description and pre-industrial simulation. Geosci. Model Dev. *10*, 2567–2590.

Marrari, M., Piola, A.R., Valla, D., and Wilding, J.G. (2016). Trends and variability in extended ocean color time series in the main reproductive area of the Argentine hake, Merluccius hubbsi (Southwestern Atlantic Ocean). Remote Sens. Environ. *177*, 1–12.

Monod, J. (1949). The growth of bacterial cultures. Annu. Rev. Microbiol. *3*, 371–394.

Oke, P.R., Griffin, D.A., Schiller, A., Matear, R.J., Fiedler, R., Mansbridge, J., Lenton, A., Cahill, M., Chamberlain, M.A., and Ridgway, K. (2013). Evaluation of a near-global eddy-resolving ocean model. Geosci. Model Dev. *6*, 591–615.

Reynolds, R.W., Smith, T.M., Liu, C., Chelton, D.B., Casey, K.S., and Schlax, M.G. (2007). Daily High-Resolution-Blended Analyses for Sea Surface Temperature. J. Clim. *20*, 5473–5496.

Ryan, J.P., Polito, P.S., Strutton, P.G., and Chavez, F.P. (2002). Unusual large-scale phytoplankton blooms in the equatorial Pacific. Prog. Oceanogr. *55*, 263–285.

Smale, D.A., Wernberg, T., Oliver, E.C.J., Thomsen, M., Harvey, B.P., Straub, S.C., Burrows, M.T., Alexander, L.V., Benthuysen, J.A., Donat, M.G., et al. (2019). Marine heatwaves threaten global biodiversity and the provision of ecosystem services. Nat. Clim. Change.

Wernberg, T., Smale, D.A., Tuya, F., Thomsen, M.S., Langlois, T.J., de Bettignies, T., Bennett, S., and Rousseaux, C.S. (2013). An extreme climatic event alters marine ecosystem structure in a global biodiversity hotspot. Nat. Clim. Change *3*, 78–82.

Zaba, K.D., and Rudnick, D.L. (2016). The 2014–2015 warming anomaly in the Southern California Current System observed by underwater gliders. Geophys. Res. Lett. *43*, 1241–1248.

Zhang, X., Oke, P.R., Feng, M., Chamberlain, M.A., Church, J.A., Monselesan, D., Sun, C., Matear, R.J., Schiller, A., and Fiedler, R. (2016). A near-global eddy-resolving OGCM for climate studies. Geosci. Model Dev. Discuss. 1–52.

Zhang, X., Church, J.A., Monselesan, D., and McInnes, K.L. (2017). Sea level projections for the Australian region in the 21st century. Geophys. Res. Lett. *44*, 8481–8491.

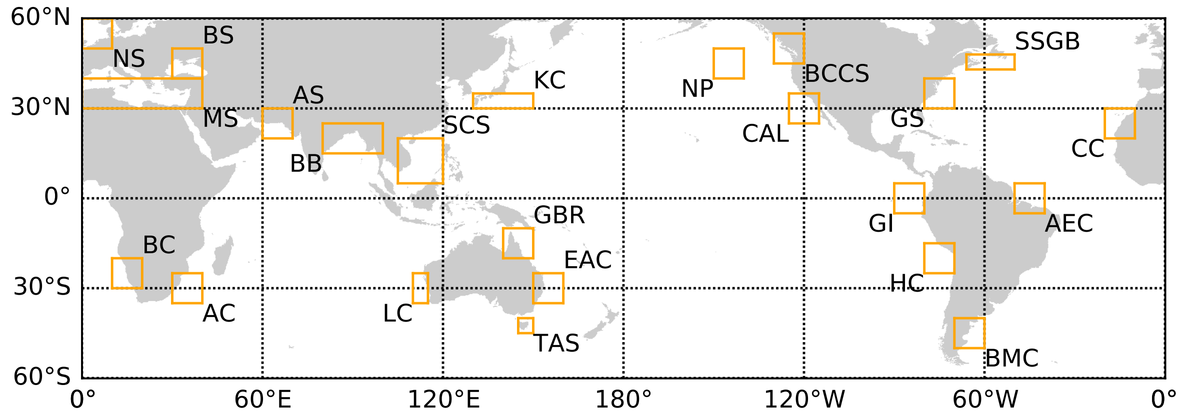

Figure 1: Locations of the 23 case-study regions. *AC: Agulhas Current, AEC: Atlantic Equatorial Current, AS: Arabian Sea, BB: Bay of Bengal, BC: Benguela Current, BCCS: British Columbia Continental Shelf, BMC: Brazil-Malvinas Confluence, BS: Black Sea, CAL: California Current, CC: Canary Current, EAC: East Australia Current, GBR: Great Barrier Reef, GI: Galapagos Island, GS: Gulf Stream, HC: Humboldt Current, KC: Kuroshio Current, LC: Leeuwin Current, MS: Mediterranean Sea, NP: Northeast Pacific, NS: North Sea, SCS: South China Sea, SSGB: Scotian Shelf and Grand Banks, TAS: Tasmania. See Table S1 for longitude and latitudinal coordinates of the regions.*

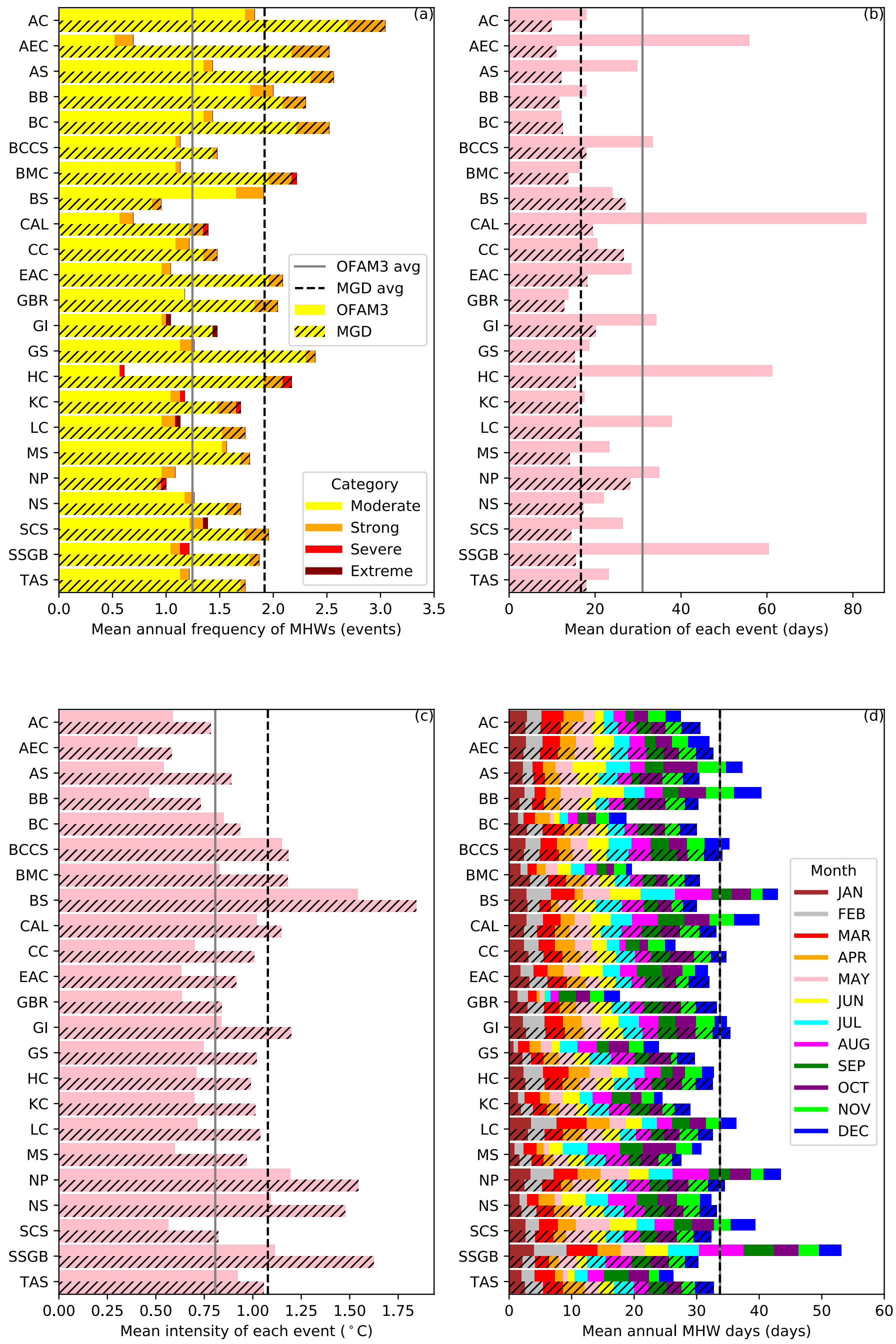

__Figure 2: Characteristics of MHWs in the 23 case-study regions based on the period 1992-2014.__ Bar graphs represent (a) how many MHW events occur, (b) how long each event lasts, (c) how much warmer the sea surface temperature is relative to the daily climatology, and (d) how many days are exposed to marine heatwaves in each region on an annual average. Bar graphs are hatched for satellite observations (MGD) to distinguish from model simulation (OFAM3). Vertical solid-grey and dashed-black lines denote the mean values of the 23 regions. In (a) and (d), colours are used in bar graphs to denote the proportion of each category and month of marine heatwave occurrence, respectively.

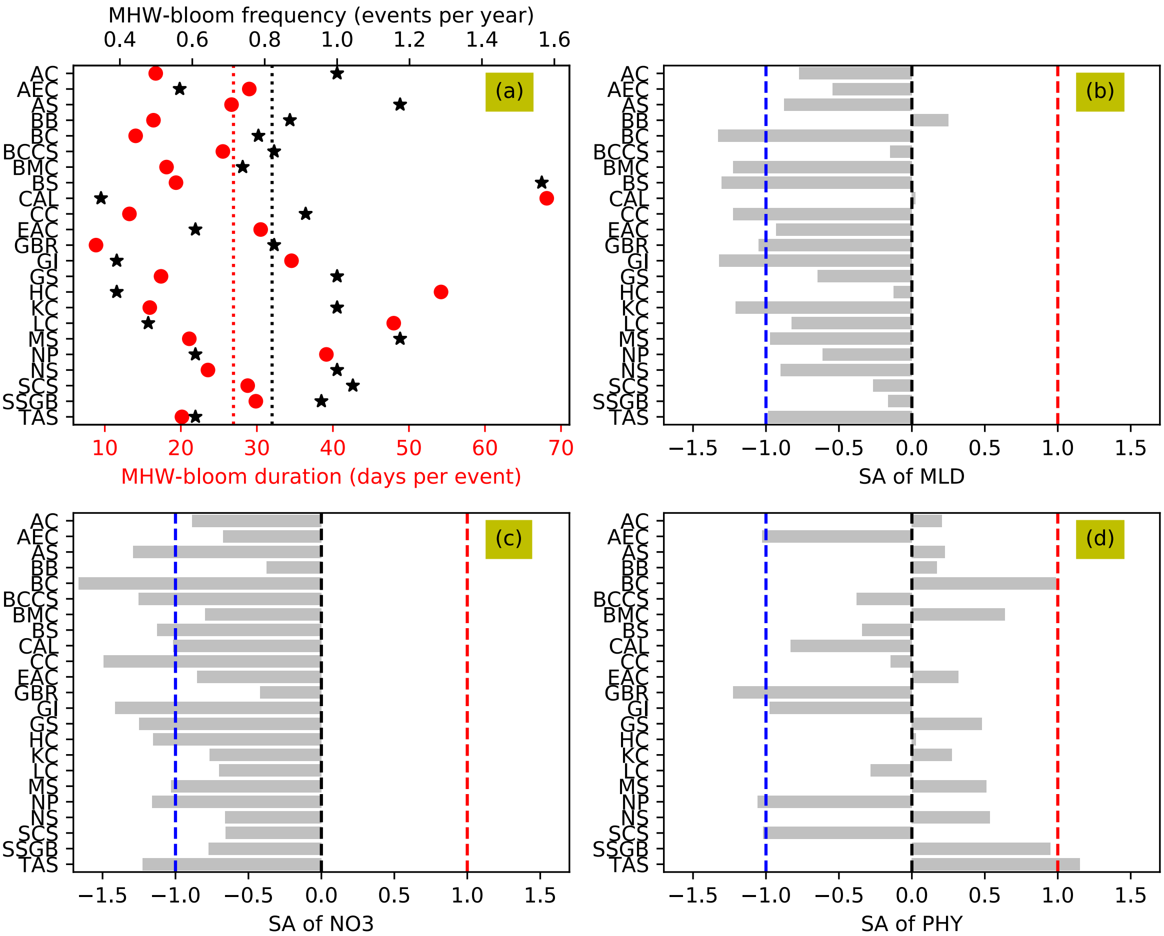

__Figure 3: Anomalies in simulated physical and biogeochemical properties during the co-occurrence of marine heatwaves and phytoplankton blooms.__ Bar graphs represent (a) mean frequency (black stars) and duration (red dots) of the marine heatwave-phytoplankton bloom co-occurrence, and mean standardized anomalies in (b) mixed layer depth, (c) sea-surface nitrate concentration, and (d) sea-surface phytoplankton biomass based on the historical experiment of OFAM3 over 1992-2014. In (a), the vertical dotted lines denote the average among the 23 regions. In (b), (c), and (d), the vertical dashed lines depict the values of -1 (blue), 0 (black), and 1 (red).

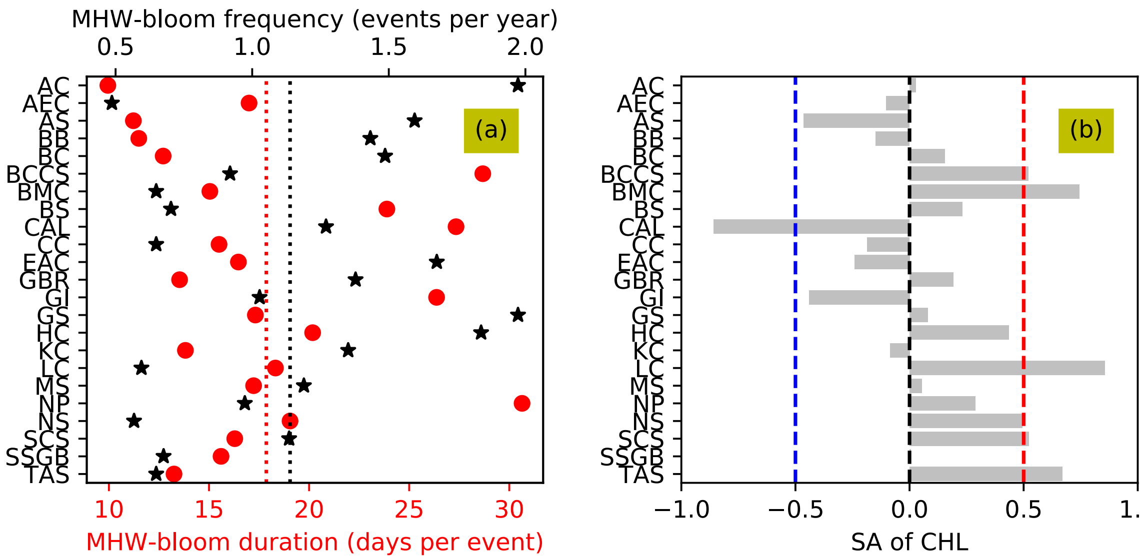

__Figure 4: Anomalies in observed sea-surface chlorophyll a concentration during the co-occurrence of marine heatwaves and phytoplankton blooms__ Bar graphs represent (a) mean frequency (black stars) and duration (red dots) of marine

heatwave-phytoplankton bloom co-occurrence and (b) mean standardized anomalies in sea-surface chlorophyll a concentration derived from satellite observations of MODIS over 2002-2018. In (a), the vertical dotted lines denote the average among the 23 regions. In (b), the vertical dashed lines depict the values of -1 (blue), 0 (black), and 1 (red).

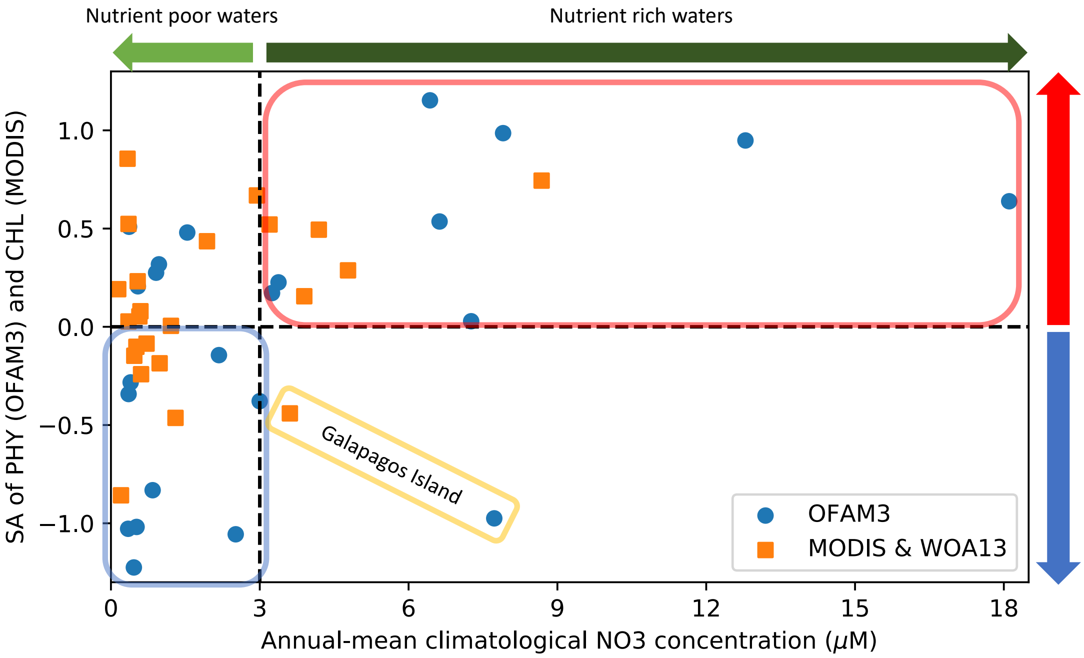

Figure 5: Relationship between phytoplankton bloom response to marine heatwaves and background nitrate concentration in the 23 study regions. *X-axis denotes the annual-mean sea-surface nitrate concentration based on the model simulation (1992-2014; OFAM3, blue) and the in situ climatology (WOA13, orange). Y-axis denotes the mean standardized anomalies of simulated sea-surface phytoplankton biomass (1992-2014; OFAM3, blue) and observed sea-surface chlorophyll a concentration (2002-2018; MODIS, orange) during the co-occurrence of phytoplankton blooms and marine heatwaves.*

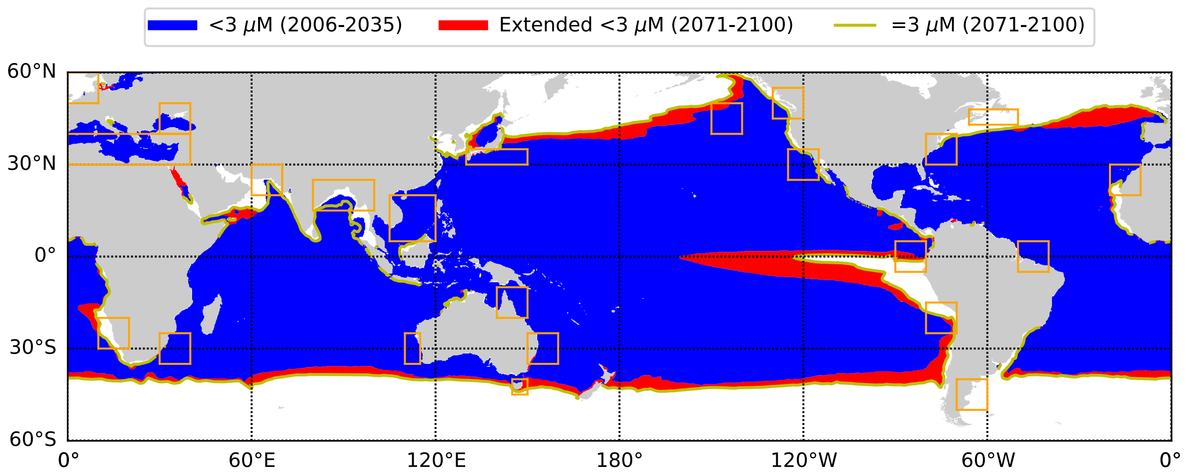

Figure 6: Projected expansion of nutrient poor waters in the twenty-first century as simulated by OFAM3. *Blue denotes the area of nitrate poor waters during 2006-2035 of the projection experiment. Nitrate poor waters are defined here as the climatological annual-mean sea-surface nitrate concentration of less than 3 μM). Red denotes the extended area of nitrate poor waters during 2071-2100. Yellow denotes the 3-μM contour during 2071-2100. Orange boxes denote the 23 study regions defined in Figure 1. The red regions will move to nutrient limited conditions under global warming and marine heatwaves will lead to reduced phytoplankton blooms.*